Supplementary Information (SI) for Journal of Materials Chemistry A.
This journal is © The Royal Society of Chemistry 2024

Supporting Information

Kirkendall effect triggered by trace Mn element on Ni-N-C catalyst for Enhanced CO_2 Electroreduction to CO

Caixia Liu,[b] Ning Liu,[a,b] Xiaoping Chen,[a] Yuzhen Zhao,[a] Jinxing Mi,[a] Zongxiang Yang,[b] Peng Wu,[a] Jianjun Chen,[a*] Junhua Li[a]

a State Key Joint Laboratory of Environment Simulation and Pollution Control, School of Environment, Tsinghua University, Beijing 100084, China.

b School of Environmental Science and Engineering, Tianjin University, Tianjin 300350， China.

*Corresponding Authors:

Jianjun Chen

Email: chenjianjun@tsinghua.edu.cn

Table of contents

Section 1: Experiment details

Materials

Zinc nitrate hexahydrate ($Zn(NO_3)_2·6H_2O$, AR), nickel nitrate hexahydrate ($Ni(NO_3)_2·6H_2O$, AR), methanol (AR, 99.5%) and Isopropyl alcohol (AR) were purchased from Sinopharm Group Chemical reagent Co., LTD. Manganese acetate tetrahydrate ($Mn(OAc)_2·4H_2O$,AR 99.0%), 2-methylimidazole ($C_4H_6N_2$, 98.0%) and Zinc acetate dihydrate ($Zn(OAc)_2·2H_2O$, 99.99%) were purchased from Macklin. Potassium bicarbonate ($KHCO_3$ AR, 99.5%) and Nafion 117 (5% in a mixture of lower aliphatic alcohols and water) were purchased from Aladdin. All purchased chemicals were used directly without further purification.

Synthesis of Mn@ZIF-8 and ZIF-8

In a typical procedure, 2.94 g $Zn(NO_3)_2·6H_2O$ and 98 mg $Mn(OAc)_2·4H_2O$ were added synchronously into 80 ml of methanol solution for stirring 30 min. Then, 3.24 g 2-methylimidazole was dissolved in 80 ml methanol solution. The metal precursor solution was added immediately into the above ligand solution and stirred constantly for 5 h. The powders (Mn@ZIF-8) were obtained by washing with methanol for several times and drying at 60 °C in a vacuum oven for overnight. ZIF-8 was prepared by similar procedures as the Mn@ZIF-8, except for the absence of $Mn(OAc)_2·4H_2O$.

Synthesis of Ni/Mn@ZIF-8 and Ni/ZIF-8

In a normal procedure, the powder of Mn@ZIF-8 (250 mg) was dispersed in n-hexane (30 ml) under ultrasound for 20 min at room temperature. After forming homogeneous solution, $Ni(NO_3)_2·6H_2O$ methanol solution (25 mg ml^{-1}, 300 μL) was injected into the mixed solution slowly under ultrasound for 10 min at room temperature. Next, the mix solution was under vigorous stirring for 1 h at room temperature in order to make the salt solution be absorbed completely. Then The powders (Ni/Mn@ZIF-8) were obtained by washing with methanol for several times and drying at 60 °C in a vacuum oven for overnight. Ni/ZIF-8 was prepared by similar procedures as the Ni/Mn@ZIF-8, but it used the Mn@ZIF-8 precursor.

Synthesis of Ni_{Mn}-N-C、Ni-N-C、N-C_{Mn} and N-C

Ni_{Mn}-N-C、Ni-N-C、N-C_{Mn} and N-C were obtained by pyrolyzing Ni/Mn@ZIF-8、Ni/ZIF-8、

Mn@ZIF-8 and ZIF-8 respectively at 910 ℃ with a rate of 5℃ min^{-1} under Ar atmosphere (150 ml/min) for 2 h.

Synthesis of Ni_{AC}-N-C

Ni_{AC}-N-C was synthesized in the same way as Ni_{Mn}-N-C, except that the $Mn(OAc)_2 \cdot 4H_2O$ was replaced by $Zn(OAc)_2 \cdot 2H_2O$.

Material characterizations

X-ray powder diffraction (XRD) was used to determine the crystal structures of the catalyst by a Bruker-AXS D8 Advance diffractometer using Cu Kα X-ray source (λ = 1.5408 Å) at the scanning rate of 10°/min from 5° to 90°, and the working voltage and current are 40 kV and 20 mA, respectively.

S4800 scanning electronic microscopy (SEM) was taken to obtain morphology of samples. The elemental distribution was visualized by energy dispersive spectroscopy mapping scan (EDS-mapping scan) on Oxford Instruments. Transmission electron microscopy (TEM) and High-resolution transmission electron microscopy (HRTEM) were performed on a JEOL-JEM-2100F instrument.

Raman spectra was recorded using a Renishaw in Via Raman microscope with a 514 nm beam from an Ar^+ ion laser. The scanning range of samples was 800~2000 cm^{-1}.

X-ray photoelectron spectroscopy (XPS) was recorded on a Thermo Scientific Escalab 250XI photoelectron spectrometer with the Al Kα (1486.6 eV) excitation 74 source under ultra-vacuum atmosphere to analyze the catalyst surface elements and their valence states. C1s peak at 284.6 eV was used to calibrate the binding energy.

The N_2 adsorption-desorption isotherms were measured at a liquid nitrogen temperature by a micromeritics ASAP 2460 instrument in the static model. Before the measurement, the catalysts were degassed at 350 ℃ for 4 h. The specific surface area was calculated by the Brunauer-Emmett-Teller (BET) equation. The pore volumes and average pore diameters were determined using the Barrett-Joyner-Halenda (BJH) method from the desorption branch of the N_2 adsorption isotherm. ICP Element (Ni and Mn content) analysis was performed using inductively coupled plasma emission spectroscopy (ICP-OES, Agilent ICPOES730).

Temperature programmed desorption of CO_2 (CO_2-TPD) profiles were used to evaluate the performance of catalysts for CO_2 adsorption. The catalyst (80 mg) was pretreated in pure He (20 mL/min) at 300℃ for 1 h. The gas stream was then switched to a pure CO_2 mixture

(20 mL/min), lasting 1 h. Subsequently, the gas stream was switched back to pure He (20 mL/min) and held for 0.5 h to purge weakly adsorbed CO_2. Finally, the temperature was increased from 50 ℃ to 500 ℃ at a heating rate of 10 ℃/min to complete desorption.

In situ attenuated total reflection surface-enhanced infrared absorption spectra (ATR-SEIRAS) measurements were carried out on Thermo Scientific Nicolet iS50 FT-IR spectrometer with VeeMAX™ III Variable Angle Specular Reflectance Accessory.

Electrochemical measurements

H-type cell:

The CO_2RR experiments were executed on a CS310M EIS Potentiostat with a H-type cell filled with 0.5 M $KHCO_3$ electrolyte. Pt foil and Ag/AgCl (saturated KCl) were used as the counter electrode and reference electrode, respectively. Nafion 117 membrane was separated the cathodic chamber and anodic before adding 0.5 M $KHCO_3$ solution. In a typical preparation procedure of the working electrode, 10 mg of samples was dispersed in a component solvent 40 μL of Nafion solution (5 wt%), 1000 μL of Isopropyl alcohol, and 960 μL of water with sonication to obtain a homogeneous ink. Then, this ink was drop-casted onto a carbon fibre paper by airbrush with catalyst loading of 0.6 ±0.1 mg cm^{-2} (Area: 1 × 1 cm^2) and Lamp dried.

Before each experiment, CO_2 (99.999%) was continuously bubbled into the catholyte for 30 minutes to form a CO_2-saturated electrolyte. The flow rate of CO_2 was kept at 20 ml min^{-1}. All potentials mentioned in the electrochemical test were converted into the reversible hydrogen electrode (RHE) scale according to the Nernst equation: E (V vs. RHE) = E (V vs. Ag/AgCl) + 0.197 + 0.0591 × pH. All the potentials were without iR corrected.

LSV and EIS curves:

Linear sweep voltammetry (LSV) was carried out in Ar or CO_2-saturated 0.5 M $KHCO_3$ electrolyte with scan rate of 10 mV s^{-1}. Electrochemical impedance spectroscopy (EIS) was recorded at -0.72 V vs. RHE in the CO_2-saturated 0.5 M $KHCO_3$ electrolyte with an amplitude of 5 mV, and the frequency range was from 0.01 kHz to 100 kHz. EIS was analyzed using the distribution of relaxation times (DRT). We mainly refer to the work of Zhao's group and used the Matlab® software DRTtools developed by the Ciucci group to calculate the DRT function.[1,2]

The evaluation of ECSA:

The ECSA of all catalysts through the double-layer capacitance (C_{dl}) of the materials, which were calculated via the CV curves with different scan rate. The CVs were conducted in the non-Faradic region between -0.14 and -0.24 V vs. RHE at scan rates ranging from 10, 15, 20, 25 to 30 mV s^{-1} for Ni_{Mn}-N-C, Ni-N-C, N-C_{Mn} and N-C catalysts, and the current at -0.19 V vs. RHE scan rates was depicted to obtain the slope (C_{dl}).

The C_{dl} values of Ni_{Mn}-N-C, Ni-N-C, N-C_{Mn} and N-C catalysts are 58.7, 33.6, 28.0 and 18.7 mF cm^{-2}, respectively. The ECSA is defined as the electrochemically active area of an electrode with 1 cm^2 of geometric area. Furthermore, We used mass-normalised $ECSA_m$ to evaluate the electrochemically active area of the catalysts:

$$ECSA_{\mathrm{m}} = \frac{\frac{C_{\mathrm{dl}}}{C_{\mathrm{s}}} \times A_{\mathrm{geo}}}{\mathrm{m}}$$

C_{dl}: Double layer capacitor, mF cm^{-2};

A_{geo}: The geometric area of the electrode,1 cm^{-2};

m: Catalyst mass at the working electrode, g;

C_S: The specific capacitance of flat electrode, the C_S is generally found to be in the range of 20~60 μF cm^{-2}. We assume that the C_S are the same for all the as-prepared M-N-C catalysts and take the value of 20 μF cm^{-2} as suggested for the carbon materials.

Products analysis of electrocatalysis

The gas products and liquid products were analyzed by gas chromatograph (GC, Agilent 7820A) equipped with flame ionization detector (FID) and thermal conductivity detector (TCD), where gases of cathode compartment were collected by an online sampling system.

Faradaic efficiencies (FE) of CO and H_2 are calculated based on the following equation:

$$FE\ (\%) = \frac{Q_{Products}}{Q_{Total}} \times 100\% = \frac{(c \times v \times P \times N \times F \times 10^{-12}) / R \times T}{I \times 60 \times 10^{-3}}$$

$Q_{Products}$: Charge of the products;

Q_{Total}: Total electric charge;

I: Total current at a potential, mA;

c: Concentration of meteorological products detected by chromatography, ppm;

v: The flow rate of CO_2, 20 sccm;

P: Atmospheric pressure at standard conditions, 101325 Pa;

N: Number of electrons transferred, 2 (CO and H_2);

F: Faraday constant , 96500 C mol^{-1};

R: Thermodynamic constant, 8.314 J/(mol·K);

T: Temperature at standard conditions, 298 K.

Quantification of the active sites

We calculate the TOF_{CO} according to the following equation:

$$TOF_{CO}(h^{-1}) = \frac{I_{co} / nF}{m_{cat} \times \omega / M_{Metal}} \times 3600$$

I_{co}: Partial current for CO, A;

n: The number of electrons transferred for CO production, which is 2 for CO;

F: Faradaic constant, 96485 C mol^{-1};

m_{cat}: The mass of catalyst on the electrode, g;

ω: Metal loading in the catalyst based on ICP-OES results;

M_{metal}: The atomic mass of Ni (55.69 g mol^{-1}).

Section2: Supporting figures and tables:

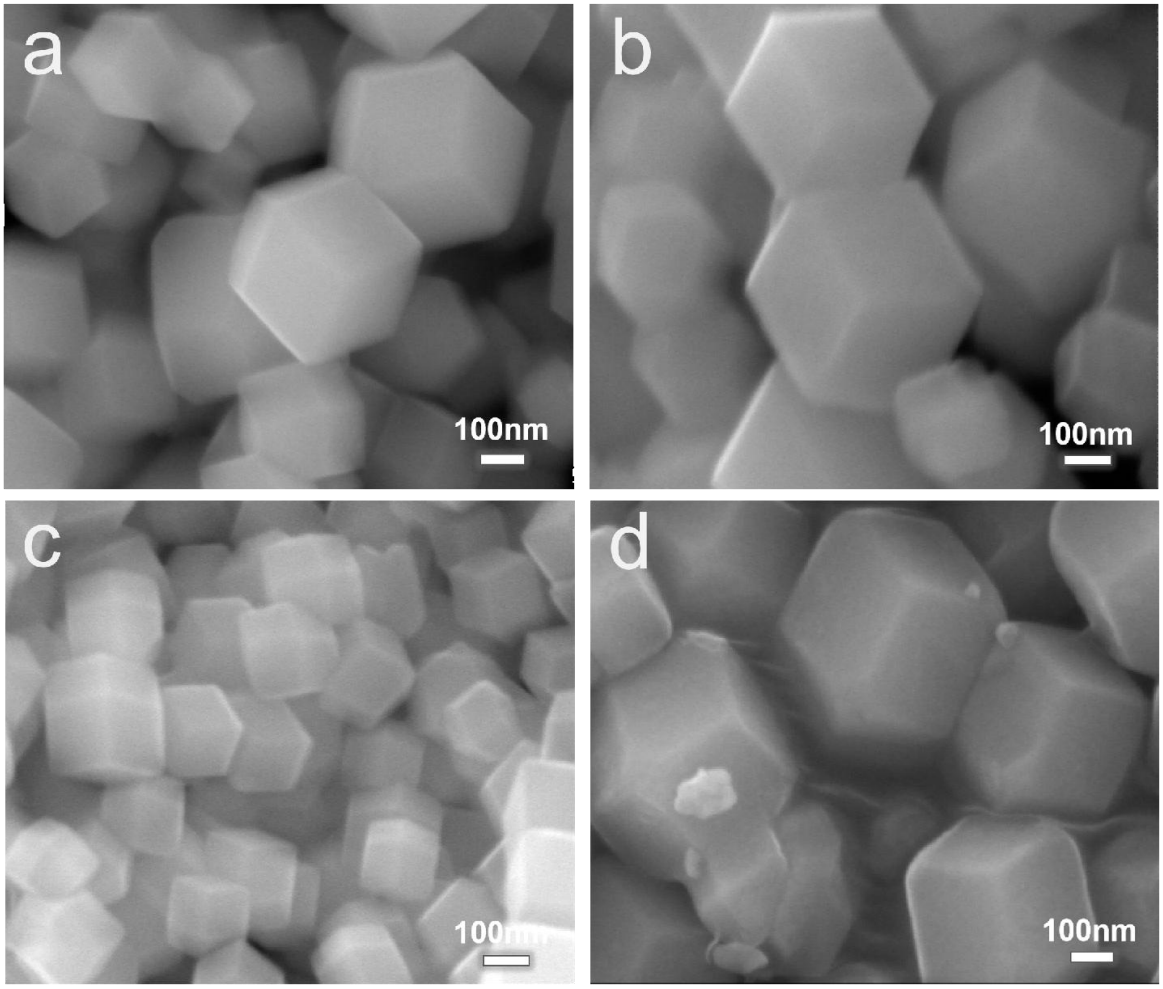

Figure S1. SEM images of (a) ZIF-8, (b) Mn@ZIF-8, (c) Ni/ZIF-8, (d) Ni/Mn@ZIF-8.

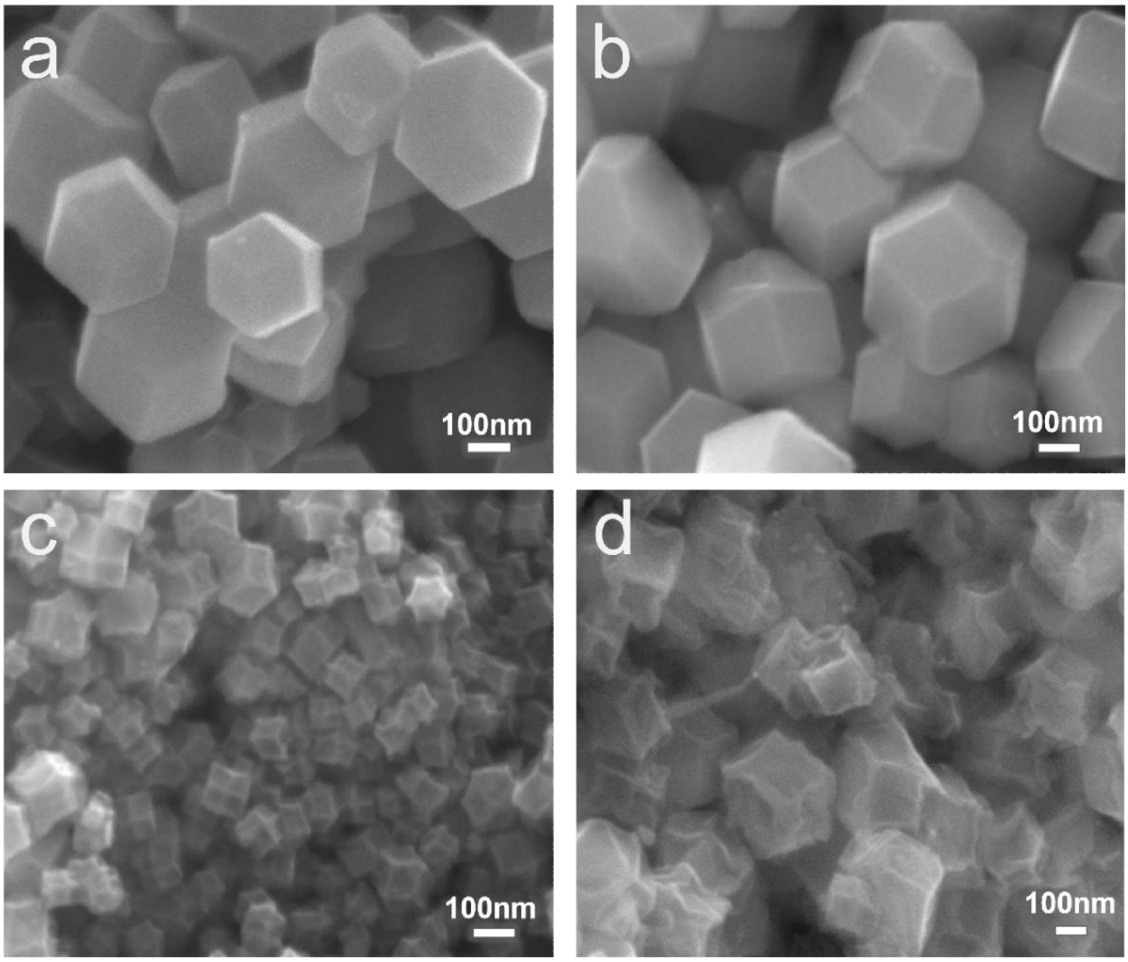

Figure S2. SEM images of (a) N-C, (b) N-C_{Mn}, (c) Ni-N-C, (d) Ni_{Mn}-N-C.

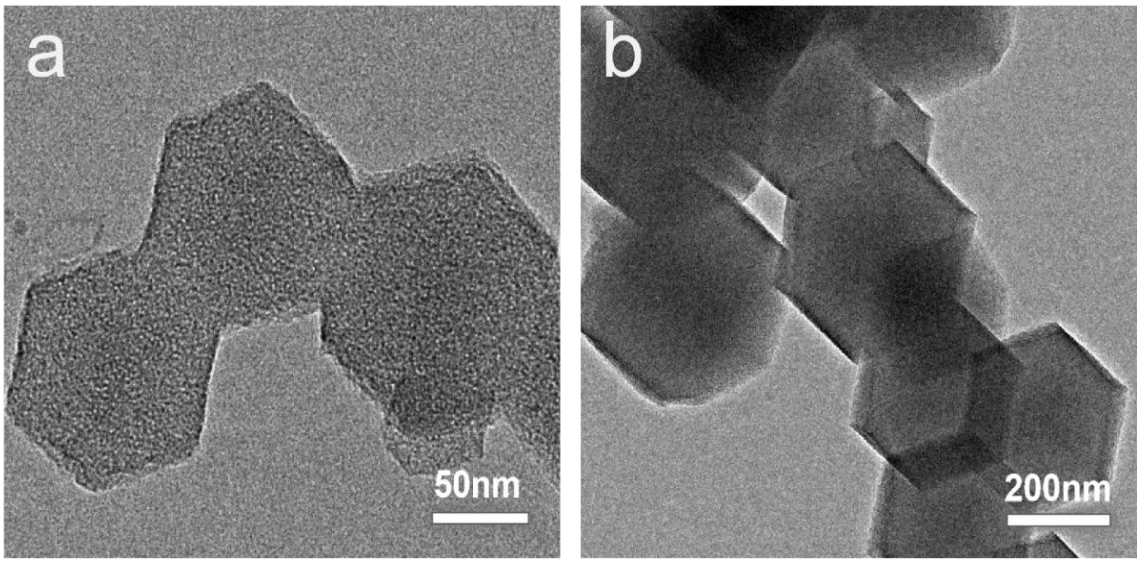

Figure S3. TEM images of (a) N-C, (b) N-C_{Mn}.

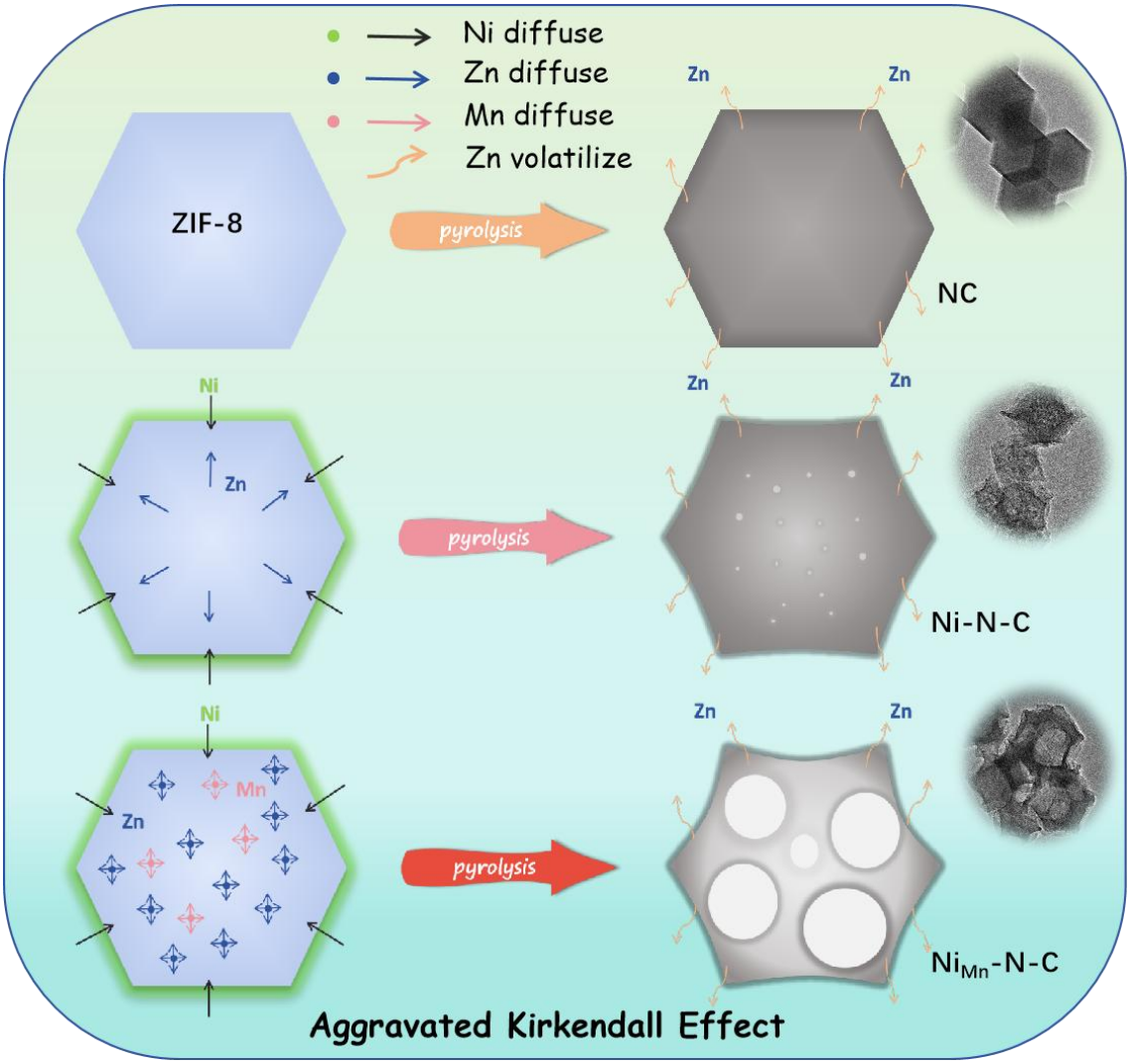

Figure S4. Schematic diagram of the formation process of the Kirkendall effect exacerbated by Mn.

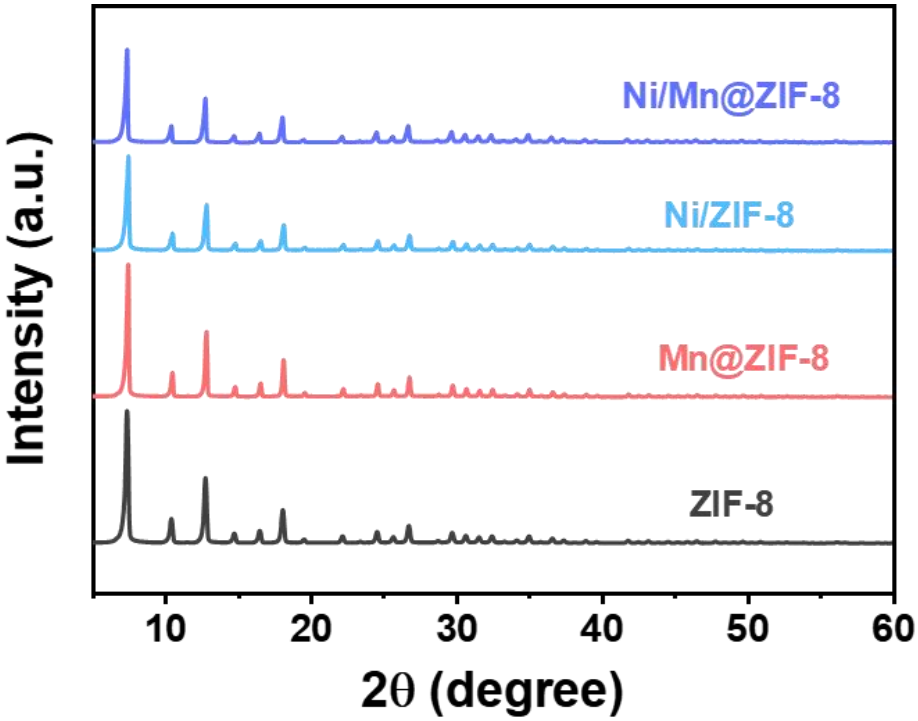

Figure S5. XRD patterns of (a) ZIF-8, (b) Mn@ZIF-8, (c) Ni/ZIF-8, (d) Ni/Mn@ZIF-8.

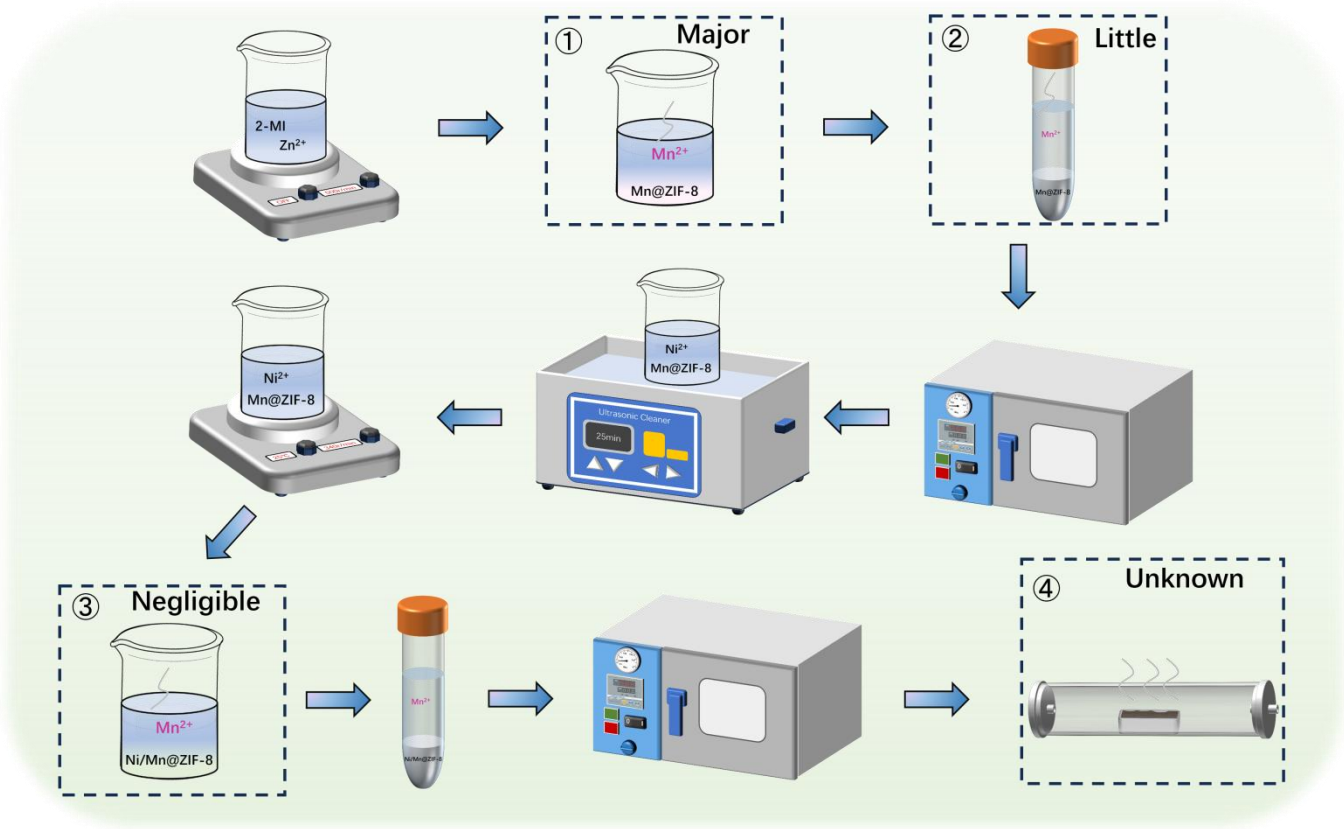

Figure S6. Schematic analysis of Mn loss during synthesis.

Since the content of Mn in the samples differed greatly from the actual dosage, we performed an elemental loss analysis of Mn, and ICP tests of Mn were carried out on the solutions of each key step of the reaction. Mn was mainly lost during synthesis in the following four steps:

①: Mn not encapsulated into the ZIF-8 cage structure during synthesis remains in solution. (Major)

②: Cleaning of Mn@ZIF-8 with Mn residue into methanol solvent. (Little)

③: Mn lost in the solvent when impregnated with Ni^{2+} elements. (Negligible)

④: Mn volatilized as other compounds during pyrolysis. (Unknown)

Manganese itself will not vaporize at 910°C. However, some compounds of manganese produced during pyrolysis may have lower thermal stability and boiling points and may decompose or volatilize at this temperature.

Total Mn	Loss of Mn	① (Major)	② (Little)	③ (Negligible)	④
21.97 mg(0.4mmol)	Mn concentration	65.51 mg/L	5.07 mg/L	0.13 mg/L	-
	Loss of quality	65.51 mg/L×0.16 L=**10.48 mg**	5.07 mg/L×0.07 L×3=**1.06 mg**	0.13×0.035 L=**0.0046 mg**	-

We also analyzed the four steps in more detail：

(1) During the synthesis of Mn@ZIF-8, a large portion of Mn was not encapsulated into the ZIF-8 cage structure, which may be related to the Mn drug we used. In this experiment we used manganese acetate tetrahydrate, and the water of crystallization may affect the coordination environment and reactivity of manganese ions to some extent. In the process of subject-object encapsulation, the crystalline water in manganese acetate tetrahydrate may interact with some groups of ZIF-8 at the early stage of the reaction or be released gradually during the reaction process, changing the local microenvironment and affecting the rate of manganese ions into the main body of ZIF-8 and the final encapsulation amount.

(2) A small portion of the dissociated Mn^{2+} may be weakly adsorbed on the surface of Mn@ZIF-8 during cleaning, and will remain in the solution during cleaning.

(3) In the case of Ni impregnation with Mn@ZIF-8, a very small amount of Ni^{2+} may be ion-exchanged with Mn^{2+} under ultrasound, but this amount is almost negligible.

(4) During the pyrolysis process, the temperature was as high as 910 ℃, and the temperature was increased at a rate of 5 ℃/min for 2 h. Under such a high temperature environment, the manganese compounds possessed a high vapor pressure, and volatilization was very likely to occur. Although we used argon with a flow rate of 150 ml/min as a protective gas throughout the pyrolysis process, due to the complexity of the pyrolysis reaction and the persistence of the high temperature, part of the manganese may still escape from the reaction system in gaseous form. For example, some manganese oxides or manganese salts with low melting points may sublimate or decompose into gaseous products at high temperatures, leading to a significant reduction of manganese content in the final product.

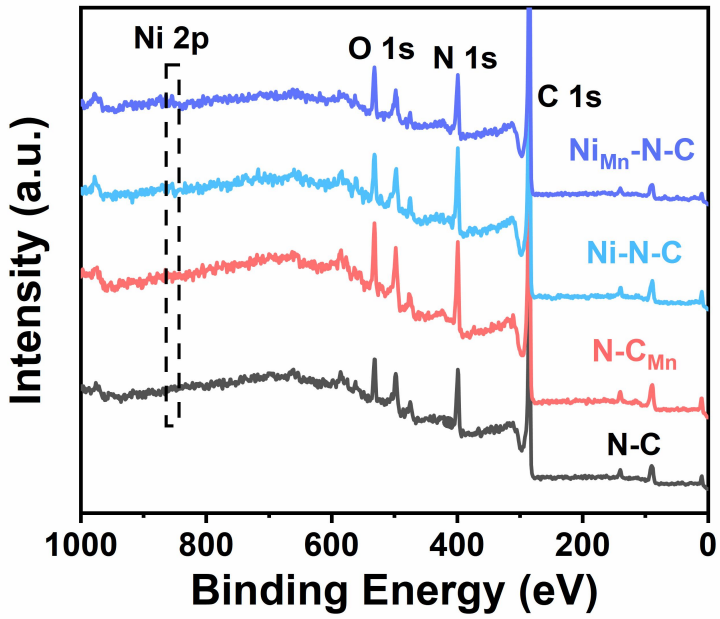

Figure S7. The XPS survey spectra of N-C, N-C_{Mn}, Ni-N-C and Ni_{Mn}-N-C.

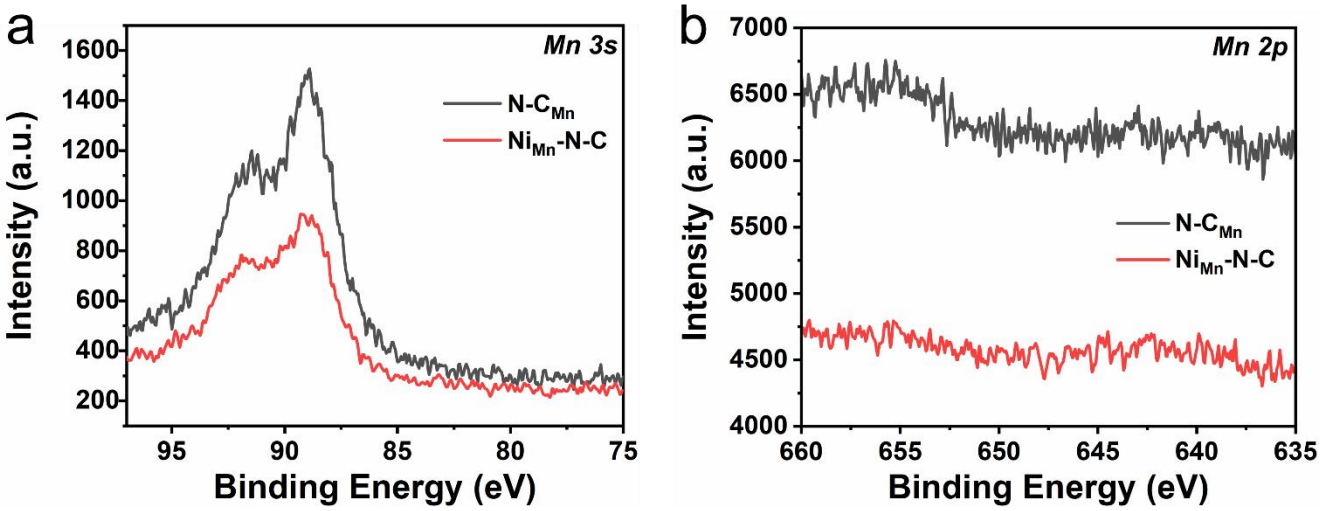

Figure S8. High resolution XPS spectra of (a) Mn 3s and (b) Mn 2p for N-C_{Mn} and Ni_{Mn}-N-C.

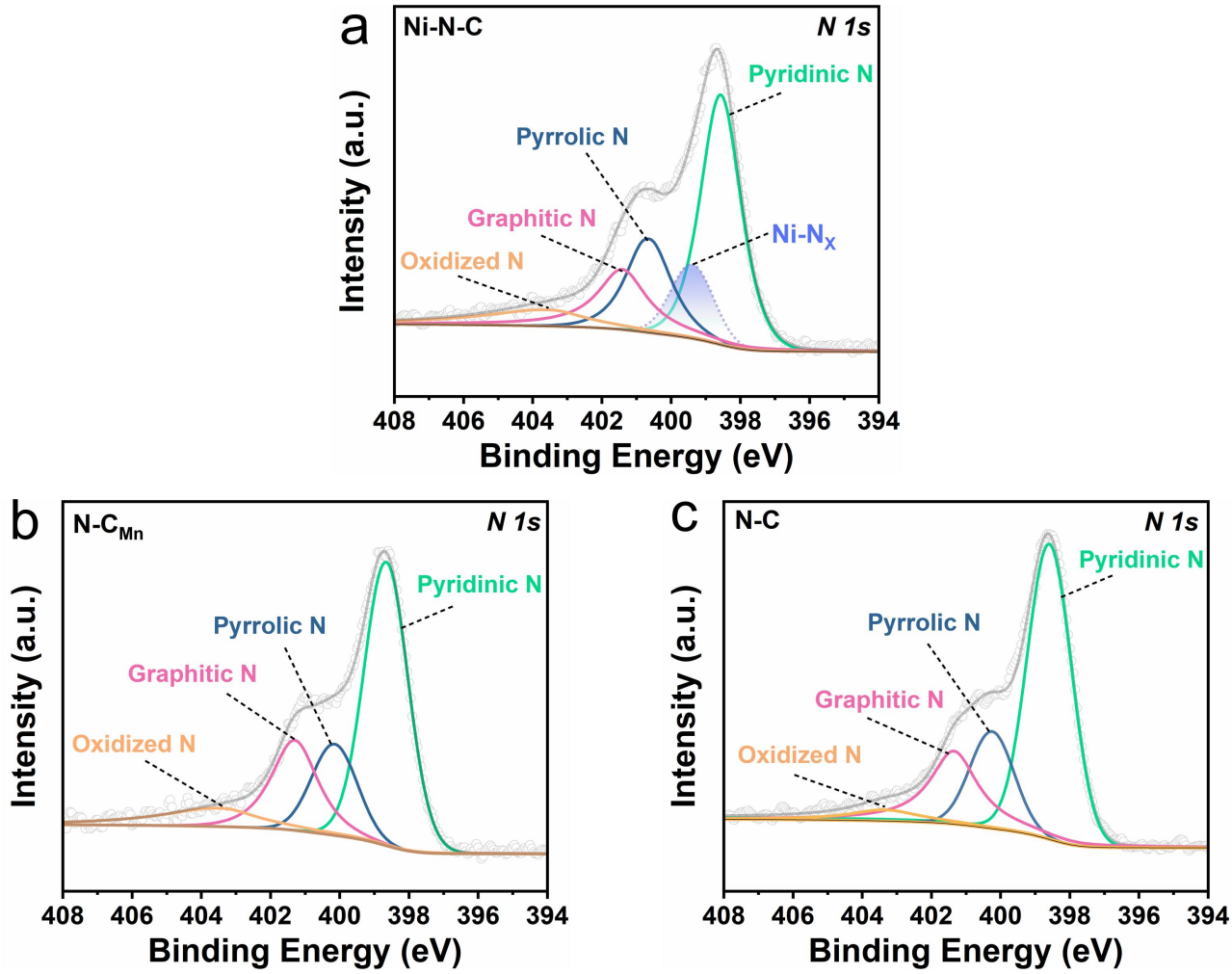

Figure S9. High resolution XPS spectra of N 1s for (a) N-C, (b) N-C_{Mn} and (c) Ni_{Mn}-N-C.

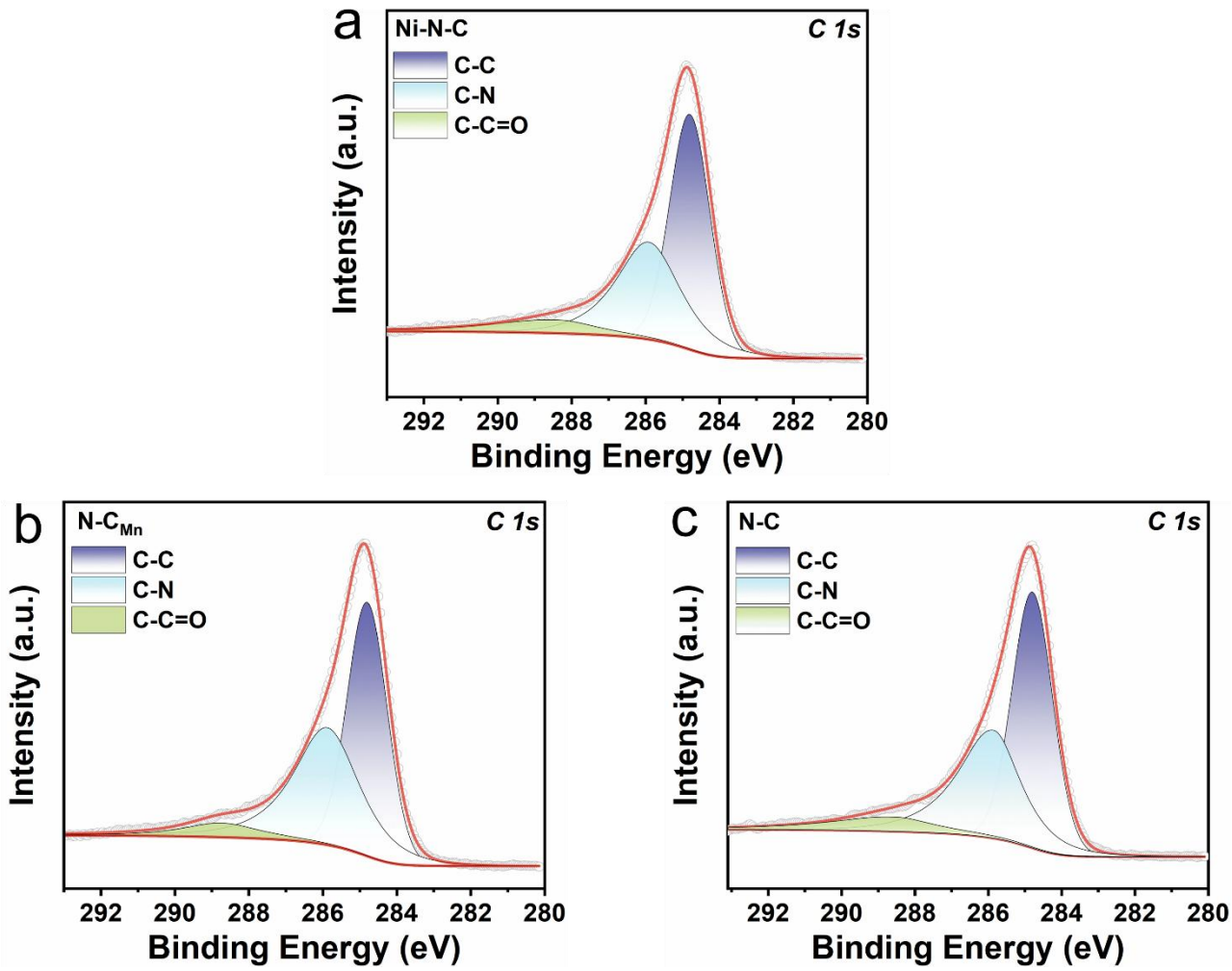

Figure S10. High resolution XPS spectra of C 1s for (a) N-C, (b) N-C_{Mn} and (c) Ni_{Mn}-N-C.

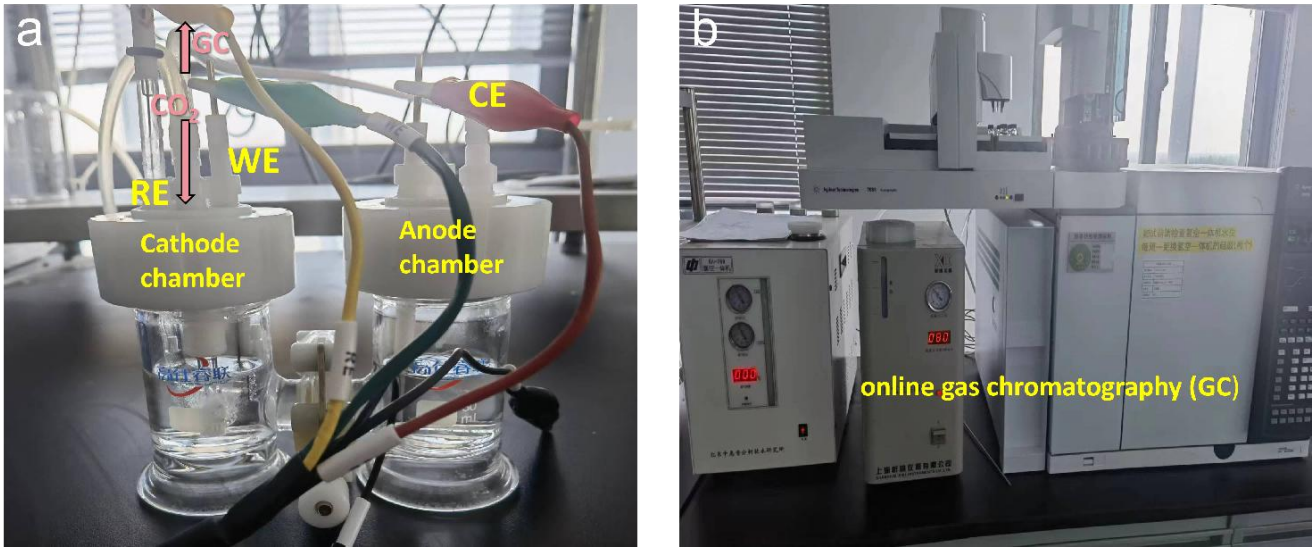

Figure S11. Photographs of (a) H-type electrolytic cell and (b) online gas chromatography.

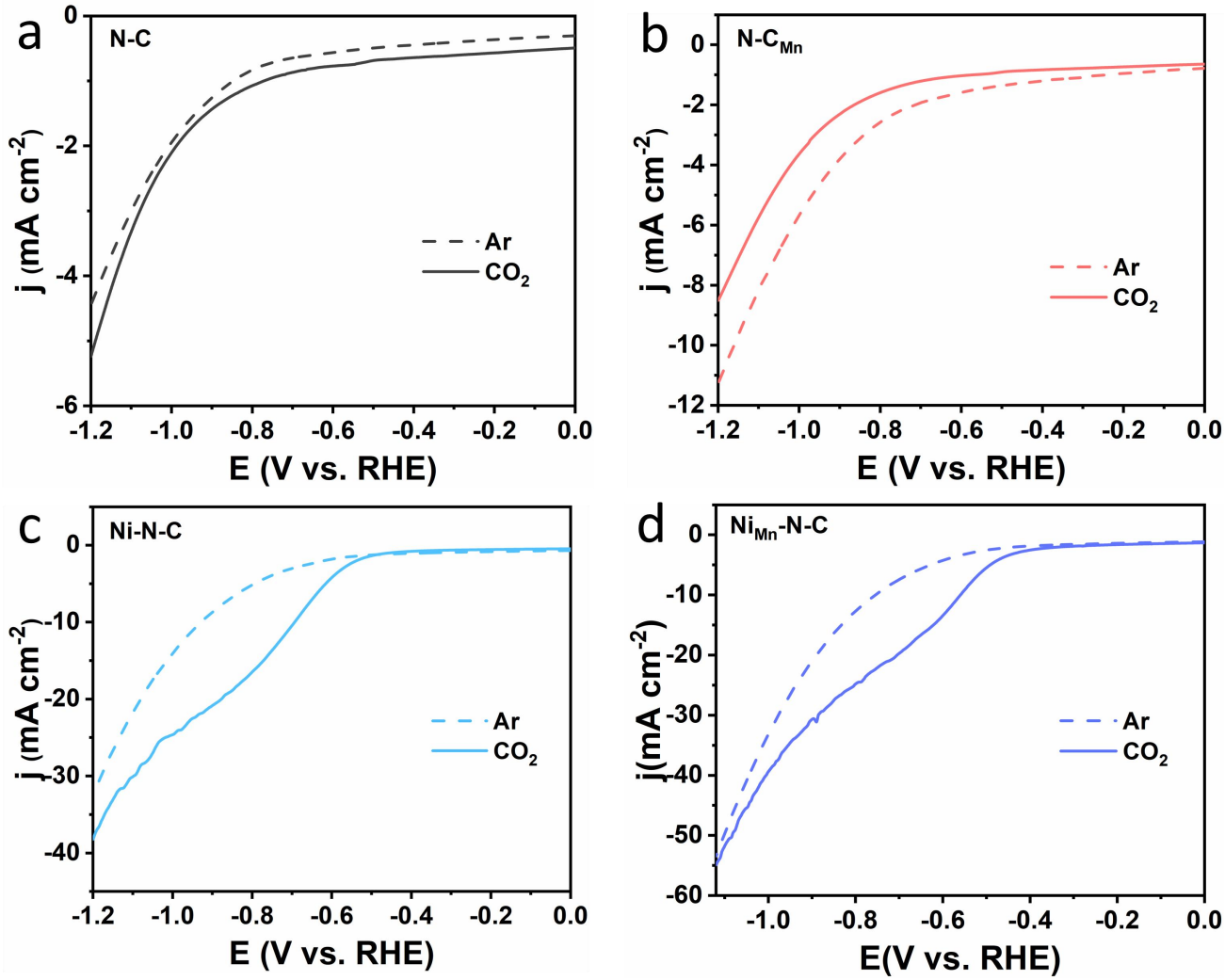

Figure S12. LSV curves of (a) N-C, (b) N-C_{Mn}, (c) Ni-N-C and (d) Ni_{Mn}-N-C in CO_2 and Ar-saturated 0.5 M $KHCO_3$.

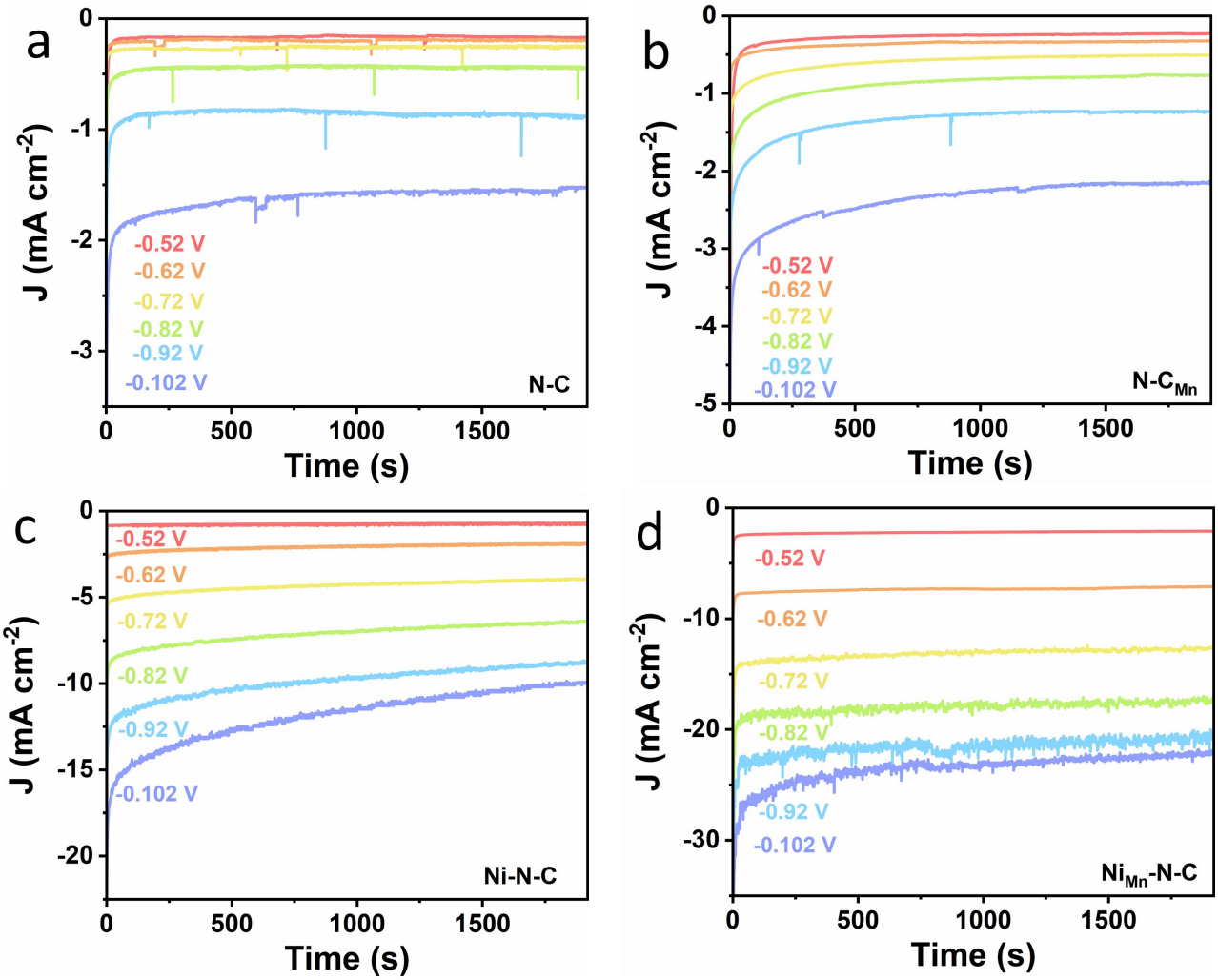

Figure S13. The chronoamperometric curves of (a) N-C, (b) N-C_{Mn}, (c) Ni-N-C and (d) Ni_{Mn}-N-C.

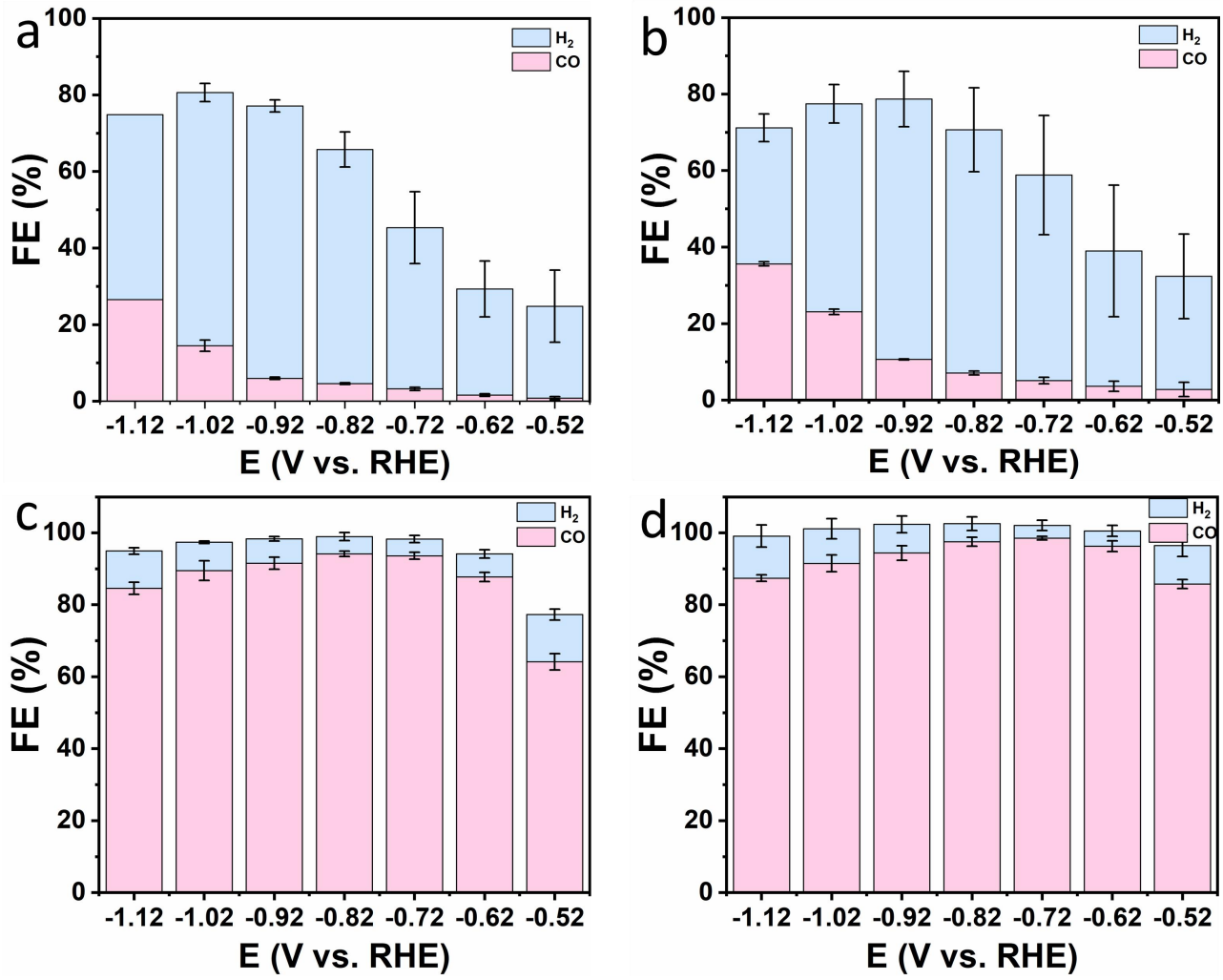

Figure S14. Faradaic efficiencies for CO (pink) and H_2 (blue) at various applied potentials of (a) N-C, (b) N-C_{Mn}, (c) Ni-N-C and (d) Ni_{Mn}-N-C.

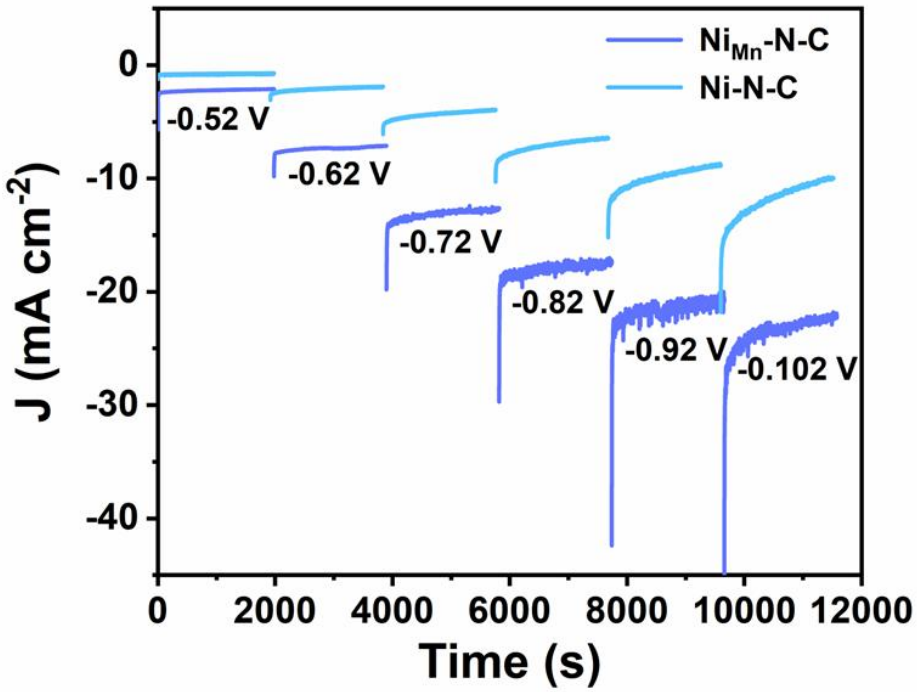

Figure S15. Comparison of electrolytic currents of Ni-N-C and Ni_{Mn}-N-C at various potentials.

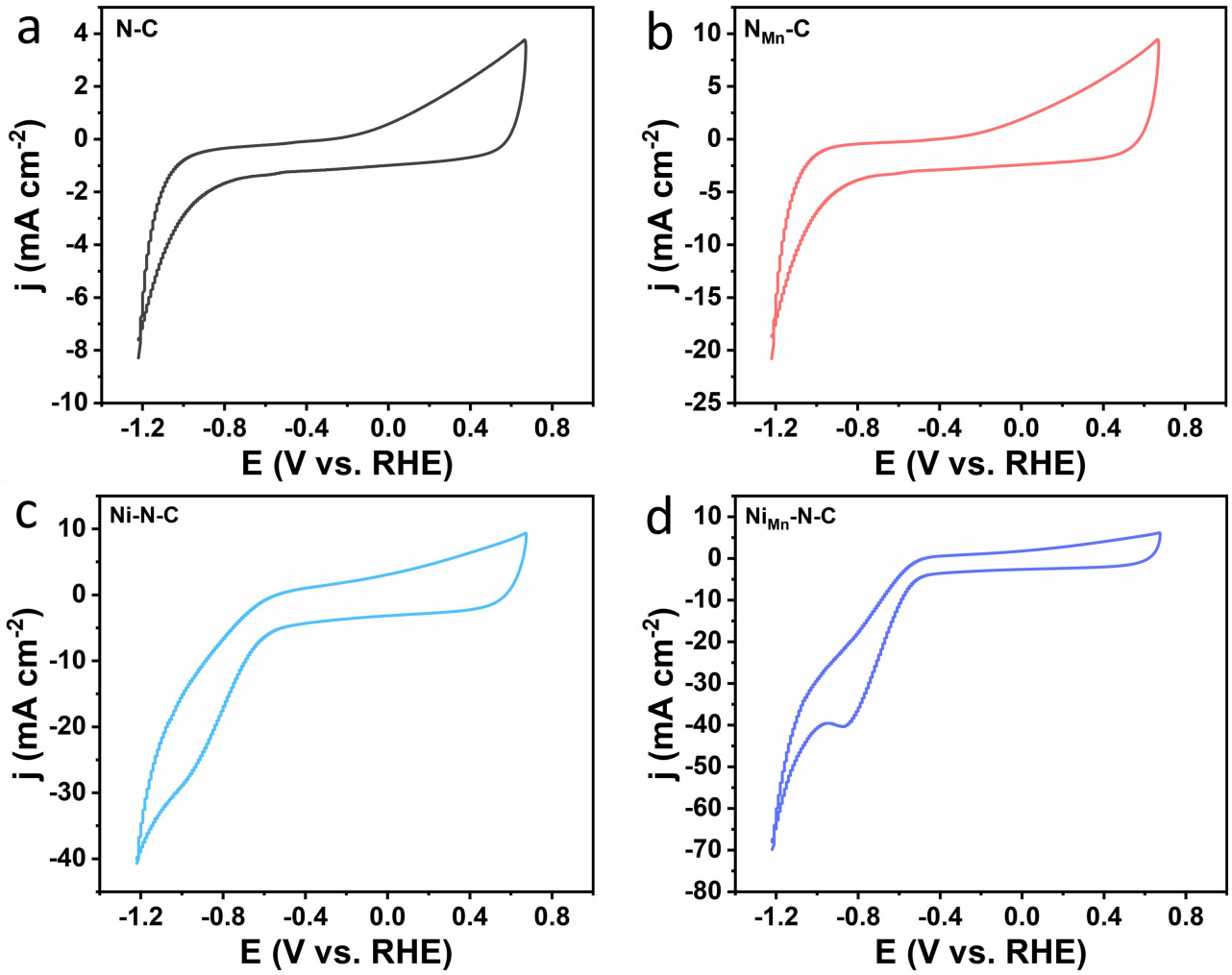

Figure S16. CV curves of (a) N-C, (b) N-C_{Mn}, (c) Ni-N-C and (d) Ni_{Mn}-N-C.

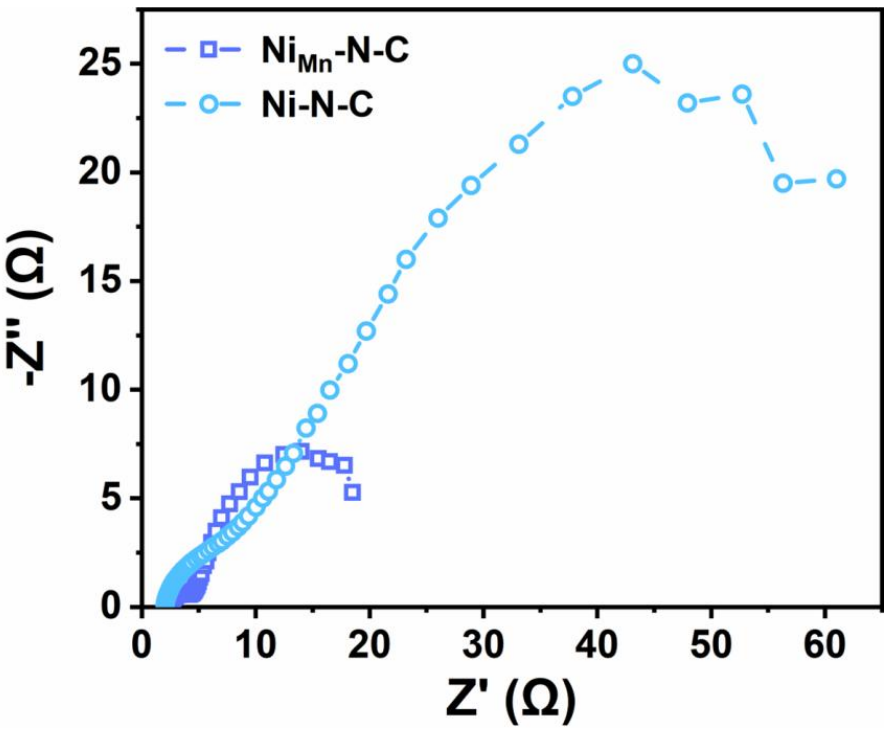

Figure S17. Raw EIS data of Ni-N-C and Ni_{Mn}-N-C.

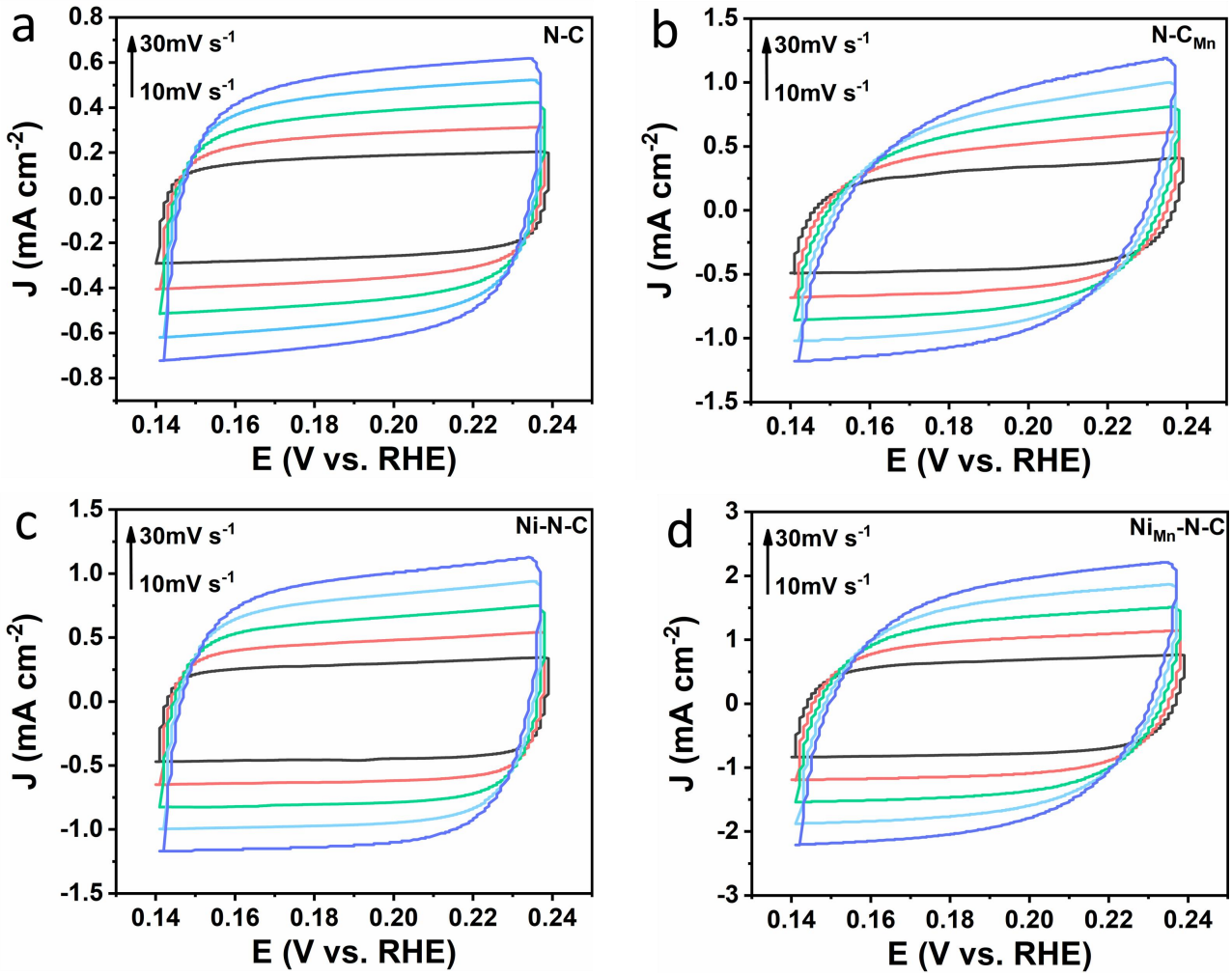

Figure S18. Cyclic voltammograms of (a) N-C, (b) N-C_{Mn}, (c) Ni-N-C and (d) Ni_{Mn}-N-C at various scan rates of 10, 15, 20, 25 and 30 mV s^{-1}.

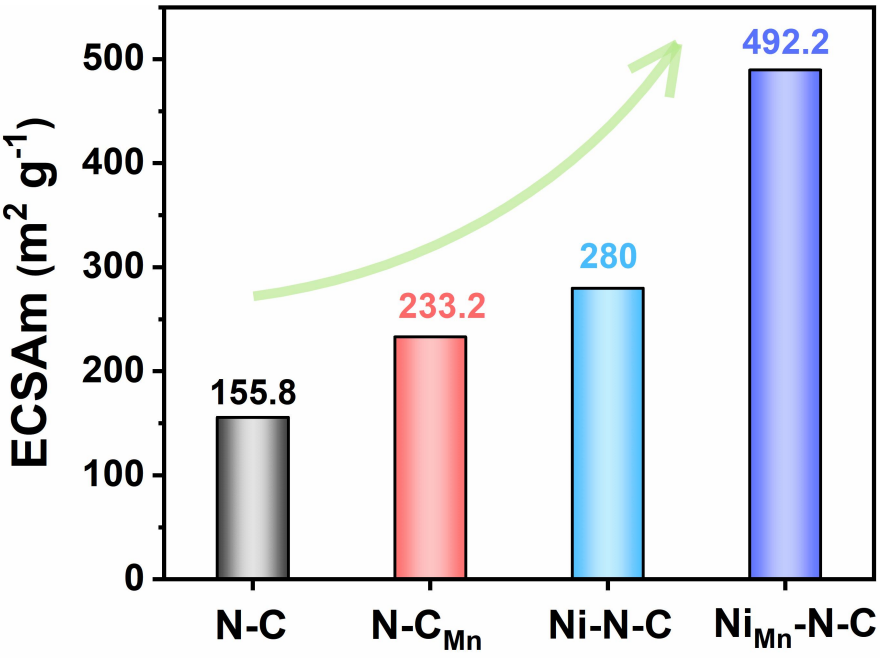

Figure S19. Mass-normalized ECSA for N-C, N-C_{Mn}, Ni-N-C and Ni_{Mn}-N-C.

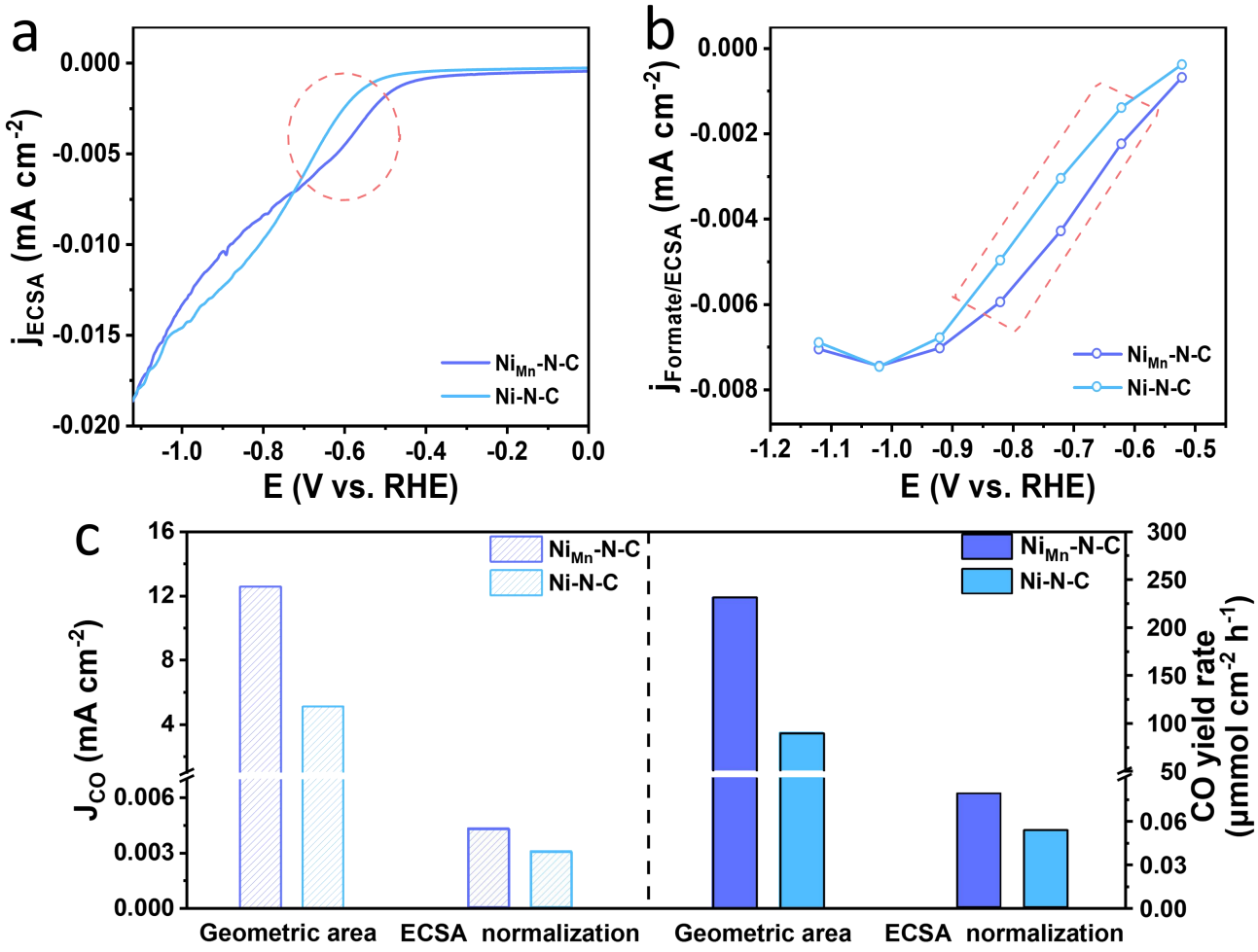

Figure S20. (a) Electrochemical area-normalised LSV curves, (b) Electrochemical area-normalised j_{CO}, (c) Comparison of CO bias current density and CO yield after electrochemical area normalisation at －0.72 V vs. RHE.

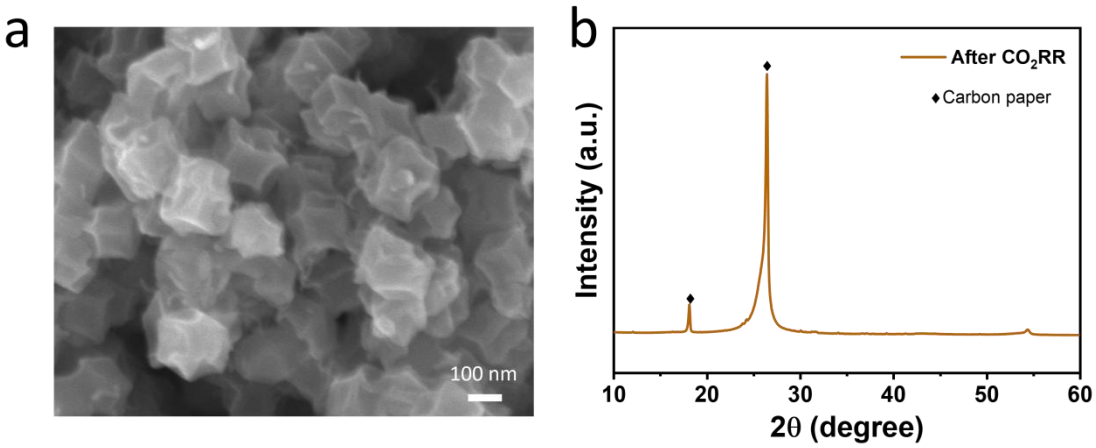

Figure S21 SEM (a) and XRD (b) images of Ni_{Mn}-N-C after CO_2RR test

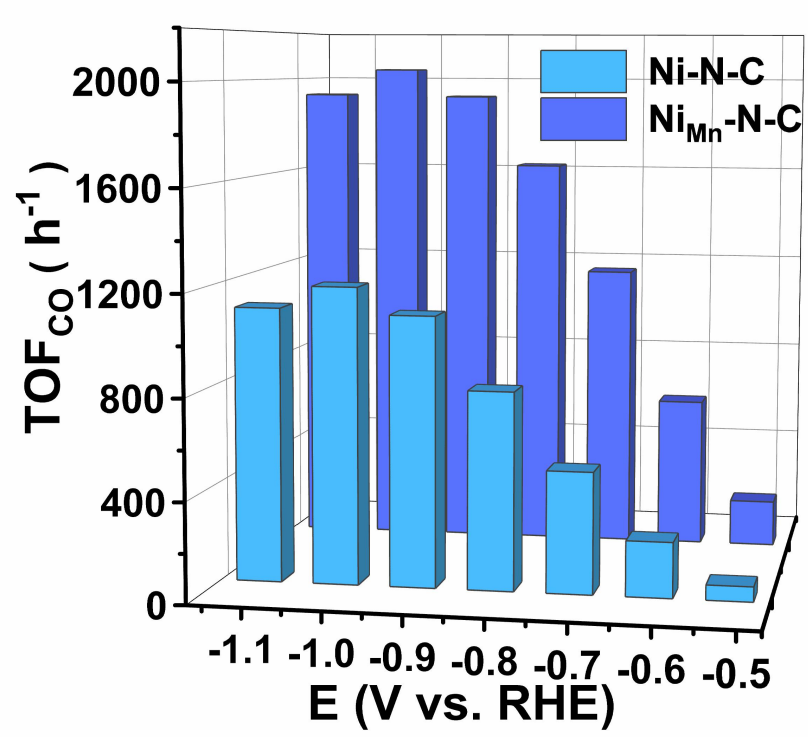

Figure S22. Calculated TOF_{CO} for N-C, N-C_{Mn}, Ni-N-C and Ni_{Mn}-N-C.

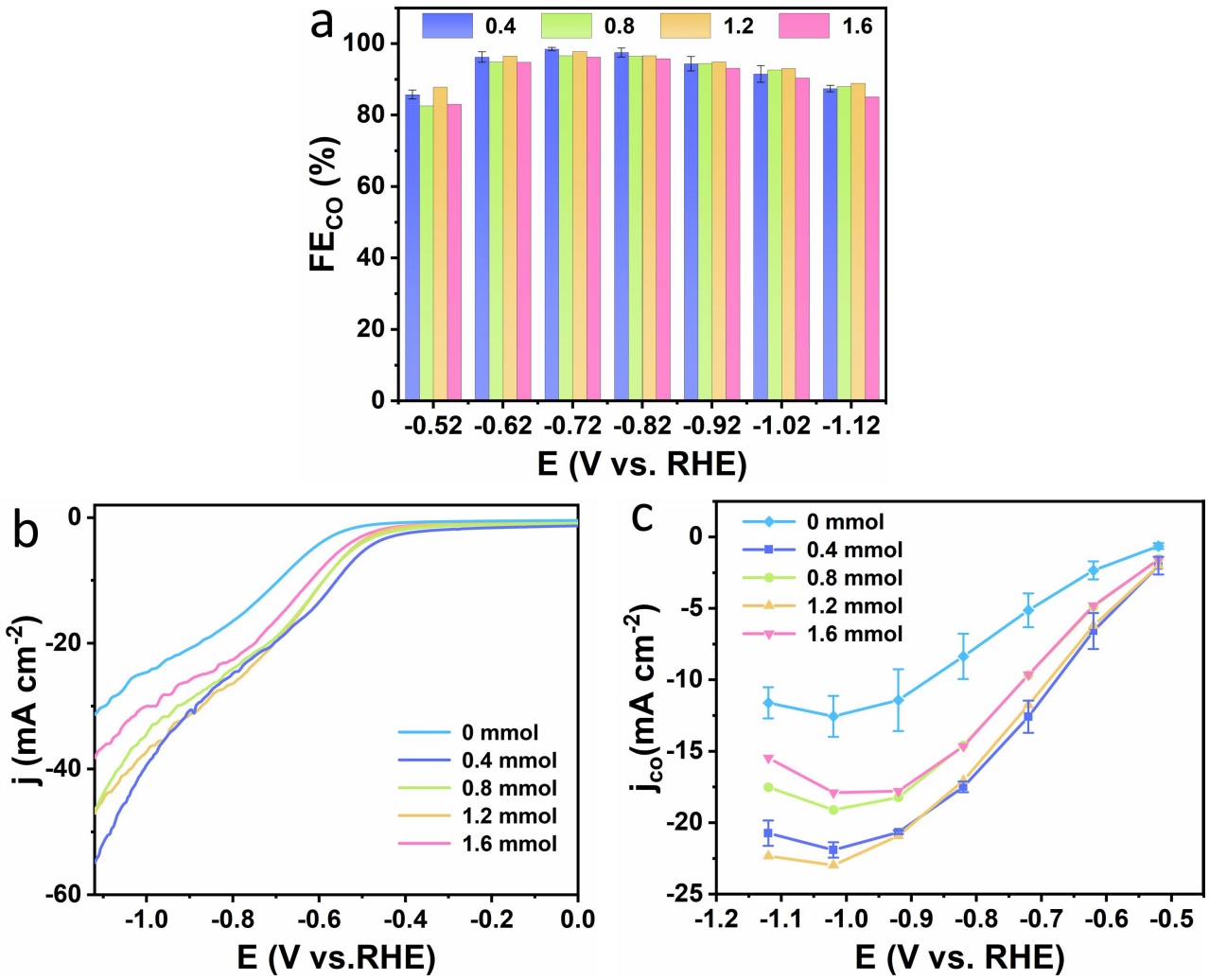

Figure S23. (a) CO Faraday efficiency, (b) LSV curves and (c) CO partial current density graphs for different amounts of Mn added.

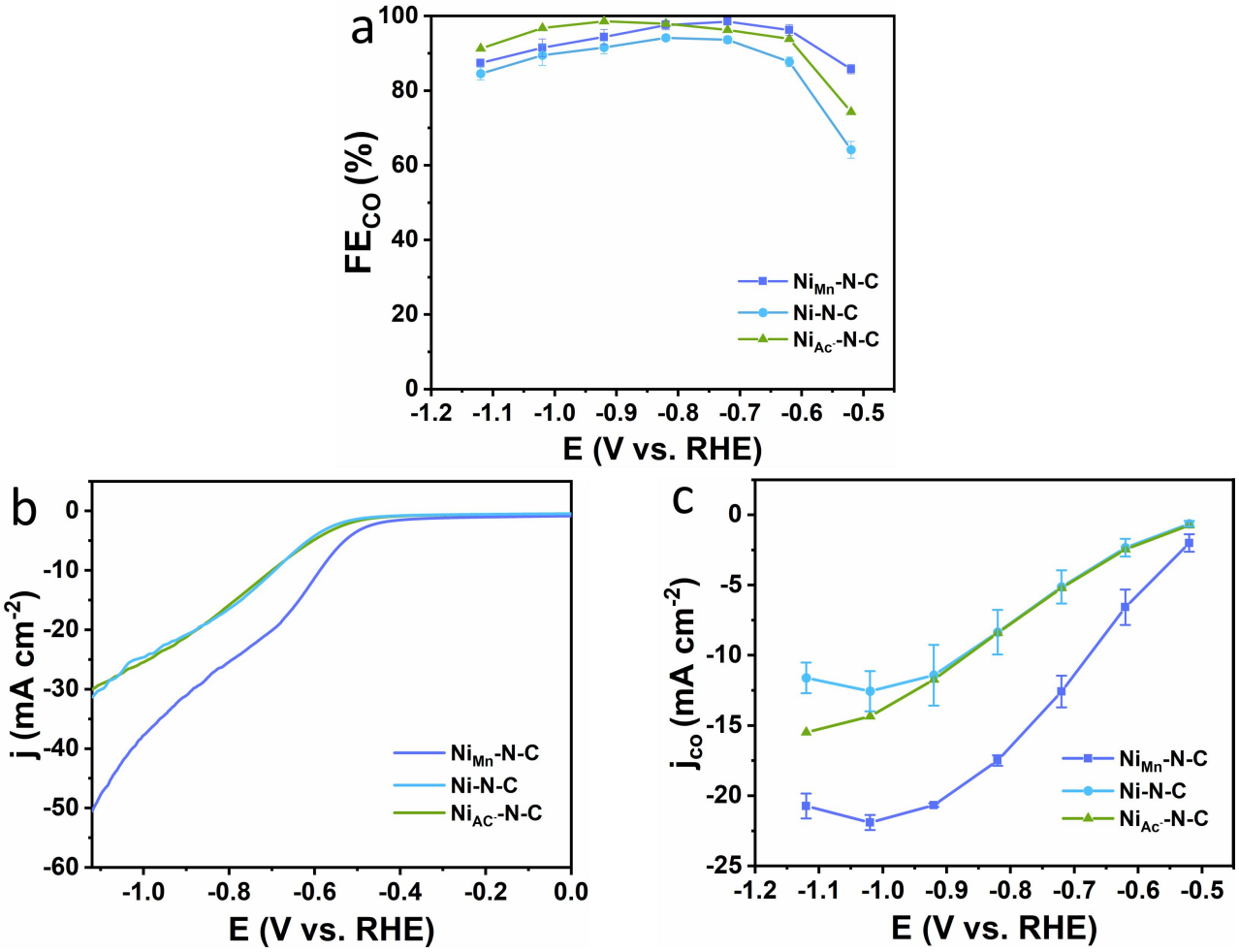

Figure S24. (a) CO Faraday efficiency, (b) LSV curves and (c) CO partial current density graphs for Ni_{Mn}-N-C, Ni_{AC}-N-C ($Mn(OAc)_2{\cdot}4H_2O$ is replaced with an equivalent amount of $Zn(OAc)_2{\cdot}2H_2O$ in the synthesis process) and Ni-N-C.

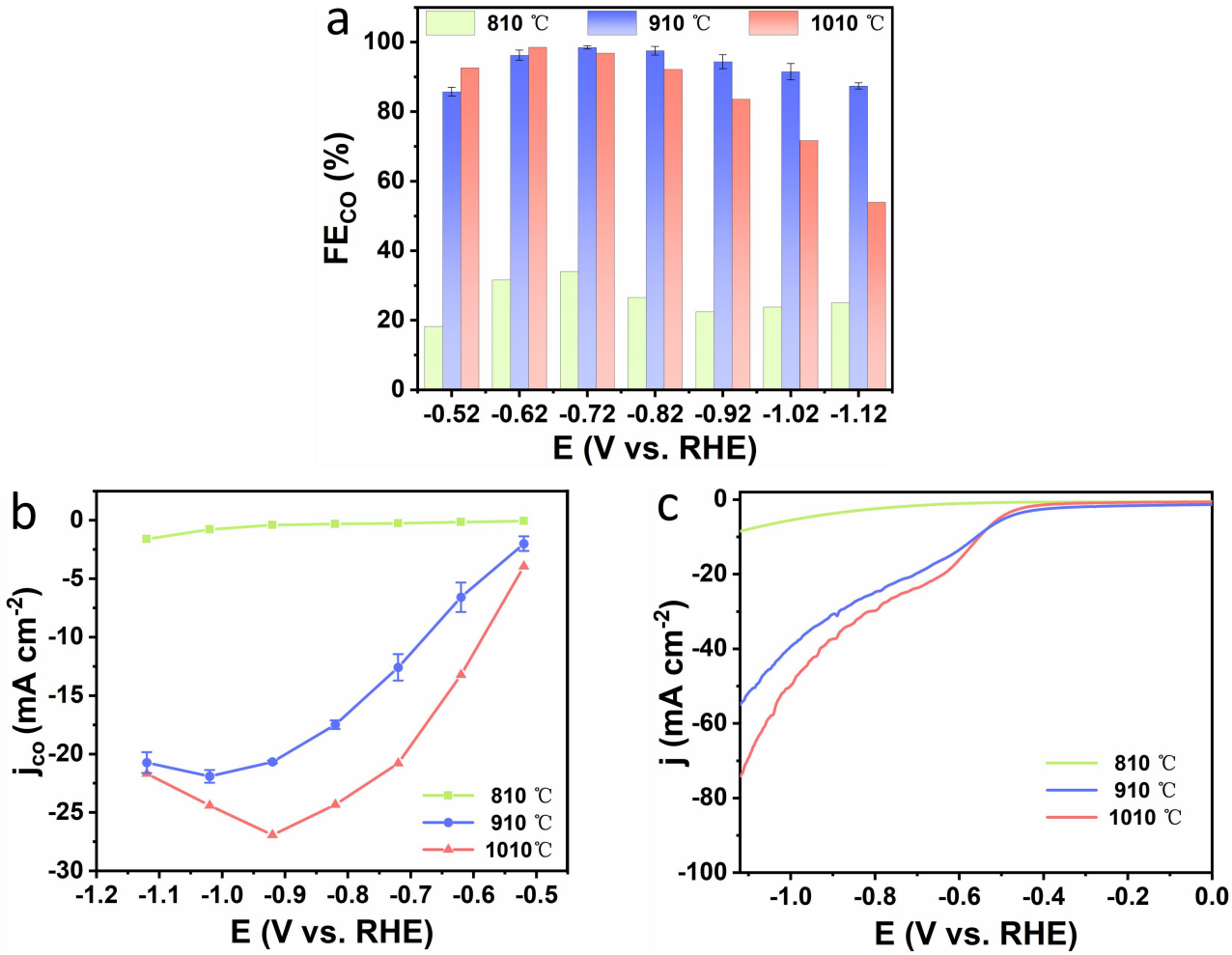

Figure S25. (a) CO Faraday efficiency, (b) LSV curves and (c) CO partial current density graphs for Ni_{Mn}-N-C pyrolyzed at different temperatures.

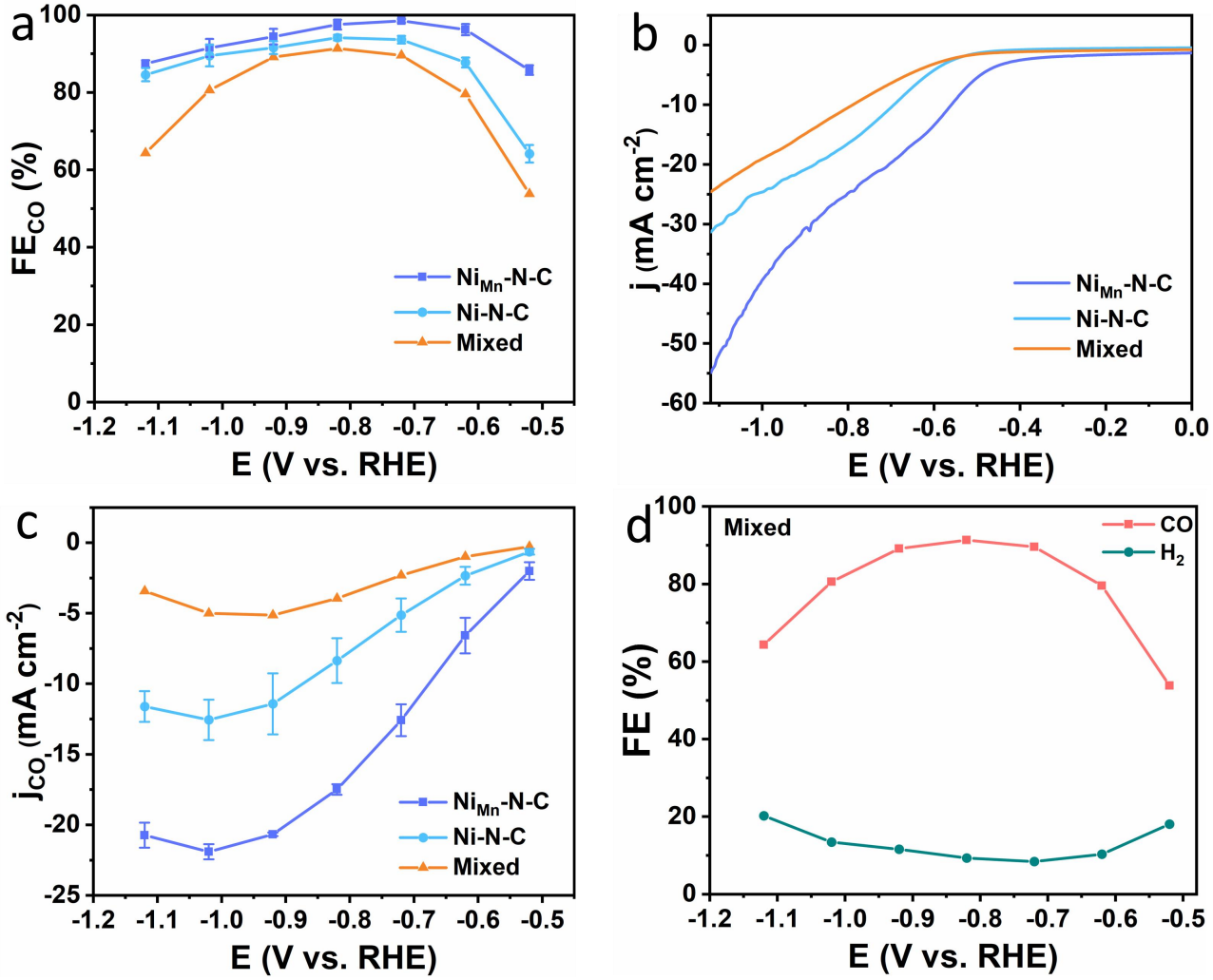

Figure S26. (a) CO Faraday efficiency, (b) LSV curves, (c) CO partial current density and (d) Total Faraday efficiency graphs for Ni_{Mn}-N-C, Ni-N-C and Mixed (physical mixing Ni-N-C and N-C_{Mn}).

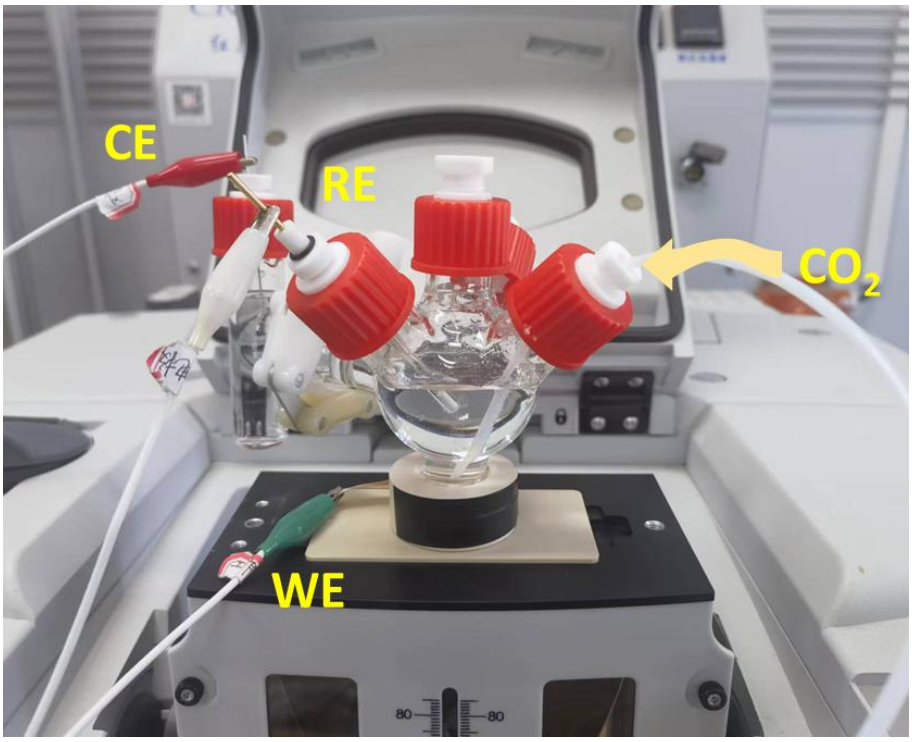

Figure S27. The digital photo of in situ ATR-SEIRAS experiments.

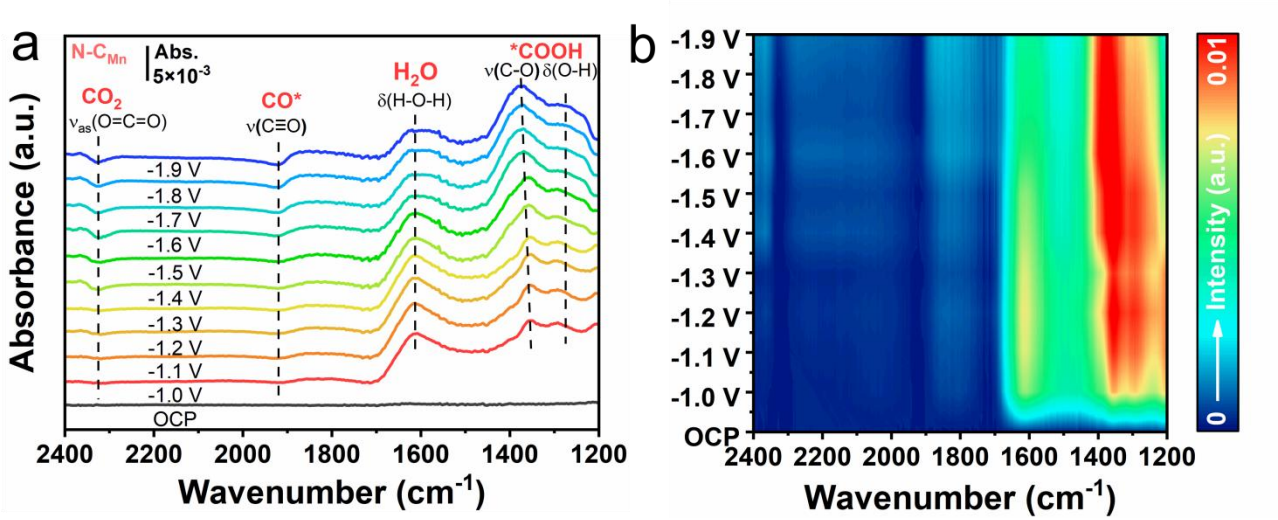

Figure S28. Potential-dependent in situ ATR-SEIRAS spectra and Contour Color Fill Map of N-C_{Mn}.

Table S1. The summaries of S_{BET} and pore volume of as-synthesized samples.

Samples	S_{BET} (m^2 g^{-1})	Total pore volume (cm^3 g^{-1})	Average pore diameter (Å)
N-C	732.70	0.412	22.51
N-C_{Mn}	890.44	0.487	21.89
Ni-N-C	688.66	0.392	22.76
Ni_{Mn}-N-C	800.09	0.493	24.66

Table S2. The weight content percentages in as-synthesized samples from ICP-OES.

Samples	Content of elements (wt%)	
	Ni	Mn
Ni-N-C	1.9265%	-
Ni_{Mn}-N-C	1.9635%	0.0071%
Ni_{Mn}-N-C-0.8	-	0.0092%
Ni_{Mn}-N-C-1.2	-	0.0202%
Ni_{Mn}-N-C-1.6	-	0.0227%

Table S3. Summary of atomic percentages determined by XPS for nitrogen species.

Sameples		N-C	N-C_{Mn}	Ni-N-C	Ni_{Mn}-N-C
Total N Content （at.%）		15.29	14.82	17.63	13.07
Relative Content %	Pyridinic-N	56.82	53.46	56.14	35.10
	Metal-N			9.89	19.81
	Pyrrolic-N	18.07	17.65	14.59	12.11
	Graphitic-N	20.66	19.71	13.01	25.53
	Oxidized-N	4.45	9.19	6.39	7.54

Table S4. Summary of atomic percentages determined by XPS for carbon species.

Sameples		N-C	N-C_{Mn}	Ni-N-C	Ni_{Mn}-N-C
Total C Content （at.%）		74.29	75.25	73.52	77.86
Relative Content %	C-C	52.86	50.22	52.6	44.89
	C-N	38.75	43.57	38.72	43.66
	O-C=O	8.38	6.21	8.68	11.45

Table S5. Electrocatalytic CO_2 reduction performance of the catalysts in the H-type cell.

Catalysts	Electrolytes	FECO	Stability	References
Ni_{Mn}-N-C	**0.5M $KHCO_3$**	**98.5% (-0.72 V)**	**38 h**	**This work**
Ni-N_3-C[3]	0.5M $KHCO_3$	95.6% (-0.65 V)	10 h	Angew. Chem. Int. Ed. 2021
NiSA-N_2-C[4]	0.5M $KHCO_3$	98% (-0.8 V)	10 h	Angew. Chem. Int. Ed. 2020
Ni_1-N-C[5]	0.5M $KHCO_3$	96.8% (-0.8 V)	10 h	Angew. Chem. Int. Ed. 2020
HP-Ni-NC[6]	0.5M $KHCO_3$	96.8% (-0.8 V)	13 h	ACS Appl.Mater. Interfaces. 2023
Ni-N_3-V[7]	0.5M $KHCO_3$	90% (-0.9 V)	14 h	Angew. Chem. Int. Ed. 2020
Ni-N_4/C-NH_2[8]	0.5M $KHCO_3$	96.2% (-0.7 V)	10 h	Energy Environ. Sci. 2021
Ni-N_X/CB[9]	0.5M $KHCO_3$	99% (-0.8V)	35 h	Applied Catalysis B: Environmental.2023
NiNG-S[10]	0.5M $KHCO_3$	97% (-0.8 V)	20 h	Angew. Chem. Int. Ed. 2021
Ni-SNC[11]	0.5M $KHCO_3$	95% (-0.8 V)	24 h	Chemical Engineering Journal. 2022
Ni-N-C[12]	0.5M $KHCO_3$	96% (-0.7 V)	40 h	Angew. Chem. Int. Ed. 2024
NiSA/PCFM[13]	0.5M $KHCO_3$	96% (-0.7 V)	14 h	Nat. Commun. 2020
NiFe-DASC[14]	0.5M $KHCO_3$	94.5% (-0.8 V)	30 h	Nat. Commun. 2021
Ni-CNC-1000[15]	0.5M $KHCO_3$	96.6% (-0.8 V)	30 h	Angew. Chem. Int. Ed. 2022

Refernce

1 Y. Zhao, Z. Shi, F. Li, C. Jia, Q. Sun, Z. Su and C. Zhao, *ACS Catal.*, 2024, 3926–3932.

2 C. Jia, Y. Zhao, S. Song, Q. Sun, Q. Meyer, S. Liu, Y. Shen and C. Zhao, *Advanced Energy Materials*, 2023, **13**, 2302007.

3 Y. Zhang, L. Jiao, W. Yang, C. Xie and H.-L. Jiang, *Angewandte Chemie International Edition*, 2021, **60**, 7607–7611.

4 Y.-N. Gong, L. Jiao, Y. Qian, C.-Y. Pan, L. Zheng, X. Cai, B. Liu, S.-H. Yu and H.-L. Jiang, *Angewandte Chemie International Edition*, 2020, **59**, 2705–2709.

5 L. Jiao, W. Yang, G. Wan, R. Zhang, X. Zheng, H. Zhou, S.-H. Yu and H.-L. Jiang, *Angewandte Chemie International Edition*, 2020, **59**, 20589–20595.

6 C. Zhou, R. Zhang, Y. Rong, Y. Yang and X. Jiang, *ACS Applied Materials & Interfaces*, DOI:10.1021/acsami.3c08187.

7 X. Rong, H.-J. Wang, X.-L. Lu, R. Si and T.-B. Lu, *Angewandte Chemie International Edition*, 2020, **59**, 1961–1965.

8 Z. Chen, X. Zhang, W. Liu, M. Jiao, K. Mou, X. Zhang and L. Liu, *Energy Environ. Sci.*, 2021, **14**, 2349–2356.

9 S. Liang, T. Zhang, Y. Zheng, T. Xue, Z. Wang, Q. Wang and H. He, *Applied Catalysis B: Environment and Energy*, 2023, **333**, 122801.

10 C. Jia, X. Tan, Y. Zhao, W. Ren, Y. Li, Z. Su, S. C. Smith and C. Zhao, *Angewandte Chemie International Edition*, 2021, **60**, 23342–23348.

11 X. Yang, J. Cheng, H. Lv, X. Yang, L. Ding, Y. Xu, K. Zhang, W. Sun and J. Zhou, *Chemical Engineering Journal*, 2022, **450**, 137950.

12 M. Wen, N. Sun, L. Jiao, S.-Q. Zang and H.-L. Jiang, *Angewandte Chemie International Edition*, 2024, **63**, e202318338.

13 H. Yang, Q. Lin, C. Zhang, X. Yu, Z. Cheng, G. Li, Q. Hu, X. Ren, Q. Zhang, J. Liu and C. He, *Nat Commun*, 2020, **11**, 593.

14 Z. Zeng, L. Y. Gan, H. Bin Yang, X. Su, J. Gao, W. Liu, H. Matsumoto, J. Gong, J. Zhang, W. Cai, Z. Zhang, Y. Yan, B. Liu and P. Chen, *Nat Commun*, 2021, **12**, 4088.

15 X. Cao, L. Zhao, B. Wulan, D. Tan, Q. Chen, J. Ma and J. Zhang, *Angewandte Chemie International Edition*, 2022, **61**, e202113918.